Tunneling anisotropic magnetoresistance in a magnetic tunnel junction with half-metallic electrodes

J. D. Burton and Evgeny Y. Tsymbal

Phys. Rev. B **93**, 024419 — Published 25 January 2016

DOI: 10.1103/PhysRevB.93.024419

Tunneling Anisotropic Magnetoresistance in a Magnetic Tunnel Junction with Half-Metallic Electrodes

J. D. Burton* and Evgeny Y. Tsymbal†

Department of Physics and Astronomy & Nebraska Center for Materials and Nanoscience, University of Nebraska, Lincoln, Nebraska 68588-0299, USA

Tunneling anisotropic magnetoresistance (TAMR) is the difference in resistance of a magnetic tunnel junction due to a change in magnetization direction of one or both magnetic electrodes with respect to the flow of current. We present results of first-principles density functional calculations of the TAMR effect in magnetic tunnel junctions with $La_{0.7}Sr_{0.3}MnO_3$ (LSMO) electrodes and a $SrTiO_3$ (STO) tunneling barrier. We find ~500% difference in resistance between magnetization in the plane and out of the plane. This large TAMR effect originates from the half-metallic nature of LSMO: when magnetization is out-of-plane spin-orbit coupling (SOC) contributions to the transmission comes only from spin-flip scattering, which is intrinsically small due to the half-metallicity. For in-plane magnetization, however, there is a large non-spin-flip SOC contribution to the conductance. The large magnitude of the effect stems from the additional fact that there is an inherent polar discontinuity between LSMO and STO which leads to quasi-localized states at the interface whose influence on tunneling is strongly dependent on the magnetization orientation.

I. INTRODUCTION

The coupling between magnetism and electronic transport properties is one of the richest veins of research not only for the depth of fundamental phenomena available, [1] but also for the potential and proven technological applications such research has produced.[2] One of the most important device structures is the magnetic tunnel junction (MTJ), consisting of two magnetic metal electrodes separated by a thin insulating barrier through which transport occurs via quantum mechanical tunneling. The key functional feature of an MTJ is the difference in resistance when the magnetizations of the two electrodes are aligned parallel or antiparallel, the so called tunneling magnetoresistance (TMR) effect.[3] TMR can be used to sense magnetic fields in, for example, magnetic data storage.[2] One important parameter which controls the magnitude of this resistance change is the spin-polarization of the magnetic electrodes and, in principle, a magnetic metal which carries current in only one spin channel (a so called half-metal) would exhibit idealized TMR: finite resistance for parallel alignment and divergently large resistance for antiparallel alignment. Several candidate half-metallic materials are known,[4] one of them being the mixed-valence manganite $La_{0.7}Sr_{0.3}MnO_3$ (LSMO).[5] Indeed, MTJs with LSMO electrodes and a $SrTiO_3$ (STO) barrier were found to exhibit a TMR up to ~1800% at low temperatures.[6]

In addition to TMR, another magnetoresistive effect is exhibited by MTJs, namely, tunneling anisotropic magnetoresistance (TAMR). TAMR is the modern extension of one of the oldest known effects that couple magnetism and electronic transport – anisotropic magnetoresistance (AMR).[7] AMR is the phenomenon whereby the electrical resistance depends on the relative direction of the magnetization with respect to the current, which in bulk ferromagnetic 3*d* transition metals amounts to changes in resistance on the order of a few percent.[8] In tunnel junctions, TAMR manifests itself as a dependence of the resistance on the direction of the magnetization of one or both of the electrodes with respect to the plane of the junction.[9] TAMR has been observed in several systems including dilute magnetic semiconductor MTJs,[10,11,12] MTJs with Fe or CoFe electrodes,[13,14,15] atomic scale magnetic break junctions,[16,17] single-molecule junctions,[18,19] and even in MTJs with an antiferromagnetic electrode.[20]

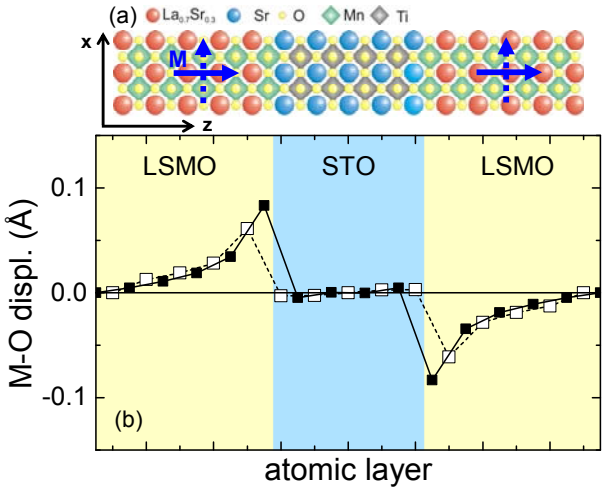

FIG. 1. (a) Schematic side view of the atomic structure of the LSMO/STO/LSMO tunnel junction. Arrows indicate the two orientations of the magnetization considered in the calculations. (b) Relaxed intra-plane metal-oxygen (M–O) displacements across the tunnel junction for M = Mn or Ti (filled symbols) and for M = $La_{0.7}Sr_{0.3}$ or Sr (open symbols).

In this work, we explore the TAMR effect in an MTJ with half-metallic electrodes, namely LSMO/STO/LSMO.

Given that the TAMR effect originates from the relativistic spin-orbit coupling (SOC) effect, i.e. the coupling of the motion of the conducing electrons with their spin magnetic moments, the question arises as to what effect this might have in a system where only one spin channel is responsible for the conduction. Using first-principles density functional calculations we find that the TAMR effect in LSMO/STO/LSMO MTJs can be very large compared to other systems, and that the magnitude of this effect originates from three important features: (i) the near perfect preservation of the electron spin during tunneling due to the half-metallicity, (ii) the well-defined orbital character of the electronic states which contribute most to tunneling and (iii) the presence of an interfacial electric field at the LSMO/STO interface due to a discontinuity of the layer-by-layer ionic structure of these two complex oxide materials.

II. STRUCTURE AND METHODS

The junction we consider consists of an STO tunneling barrier with LSMO as both left and right electrodes. The layers are stacked along the [001] direction of the conventional pseudo-cubic perovskite cell, assuming the typical AO-BO$_2$ stacking sequence (see Fig. 1a). We treat the La-Sr substitutional doping using the virtual crystal approximation where the A-site of the manganite is occupied by an atom with non-integer atomic number, reflecting the different valence of La and Sr.[21,22]

Calculations are performed using the plane-wave pseudopotential code package Quantum-ESPRESSO.[23] The supercell consists of 9.5 unit cells of LSMO and 4.5 unit cells of STO. The STO barrier layer is terminated by SrO on both sides. The exchange-correlation functional is treated in the generalized gradient approximation (GGA).[24] The in-plane lattice constant of the supercell is constrained to the calculated value for bulk cubic $SrTiO_3$, a = 3.937Å, to simulate epitaxial growth on a $SrTiO_3$ substrate. Self-consistent calculations are performed using an energy cutoff of 500 eV for the plane wave expansion and an 8×8×1 Monkhorst-Pack grid for k-point sampling. Atomic relaxations in the absence of SOC are performed until the Hellmann-Feynman forces on each atom became less than 20 meV/Å. Further relaxations in the presence of SOC are neglected.

Figure 1(b) shows the metal cation shift perpendicular to the atomic planes with respect to their intra-planar O neighbors. The polar displacements in the layers nearest to the interfaces originate from the electrostatic mismatch between the LSMO, which consists of formally charged $(La_{0.7}Sr_{0.3}O)^{0.7+}$ and $(MnO_2)^{0.7-}$ layers, whereas the STO has uncharged $(SrO)^0$ and $(TiO_2)^0$ layers. Thus both interfaces are $(MnO_2)^{0.7-}/(SrO)^0$ terminated, leading to a net electric field pointing into the STO. The electric field is screened by (i) the depletion of electrons in the metallic LSMO and (ii) the development of polar lattice displacements pointing into the interface, as shown in Fig. 1(b).[25] This incompletely screened electric field plays an important role in the TAMR effect in this system, as will be discussed below.

The conductance per unit cell area is given by the Landauer-Büttiker formula

$$G_\sigma = \frac{e^2}{h}\sum_{\mathbf{k}_\parallel} T_\sigma(\mathbf{k}_\parallel)\,, \qquad (1)$$

where $T_\sigma(\mathbf{k}_\parallel)$ is the transmission probability of an electron at the Fermi energy with spin σ and Bloch wave vector $\mathbf{k}_\parallel = (k_x, k_y)$. The tunneling transmission is calculated using a general scattering formalism [26] adapted to handle ultrasoft pseudopotentials[27] and spin-orbit coupling[28] as implemented in the Quantum-ESPRESSO package.[23] The structure depicted in Fig. 1(a) is considered as a central scattering region attached on both sides to semi-infinite LSMO leads. Matching the wave functions of the scattering region at the interfaces to the propagating states in the LSMO yields transmission coefficients. The two-dimensional Brillouin zone (2DBZ) is sampled using a uniform 100×100 $\mathbf{k}_\parallel$ mesh.

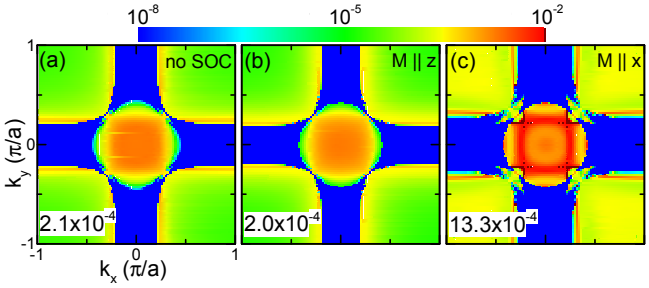

FIG. 2. The $\boldsymbol{k}_\parallel$-resolved transmission in the 2D Brillouin zone in the absence (a) and presence (b,c) of spin-orbit coupling for magnetization perpendicular (b) and parallel (c) to the plane of the layers. The integrated total conductance G is given in the lower-left corner of each plot (in units of e^2/h per unit-cell area). Note that the color scale for transmission is logarithmic.

III. RESULTS

The transmission distribution in the absence of SOC is shown in Fig. 2(a). In this case, due to the half-metallic nature of the electrodes, the minority-spin transmission is zero throughout the entire 2DBZ and therefore Fig. 2(a) corresponds to only the majority spin. The blue areas with zero transmission reflect the regions where there are no available conducting states in the LSMO electrodes, consistent with the projection of the Fermi surface along the transport direction. As seen from Fig 2(a), most of the total transmission is localized inside a circular region surrounding $\boldsymbol{k}_\parallel$ = 0. When SOC is included and magnetization is assumed parallel to the transport direction (**M** || **z**), as shown in Fig. 2(b), there are no

significant changes in the transmission profile as compared to that in the absence of SOC. This is also reflected in the total transmission which remains essentially unchanged.

When magnetization is perpendicular to the transport direction (**M** || **x**), as shown in Fig. 2(c), most of the transmission is again localized within the circular region surrounding $\boldsymbol{k}_{\|} = 0$. In this case, however, there is a distinct square-like feature with strongly enhanced transmission. As a result, the total conductance (G_x) for **M** || **x** is much larger than the total conductance (G_z) for **M** || **z** resulting in a sizable TAMR = $(G_x - G_z)/G_z$ = 531%.

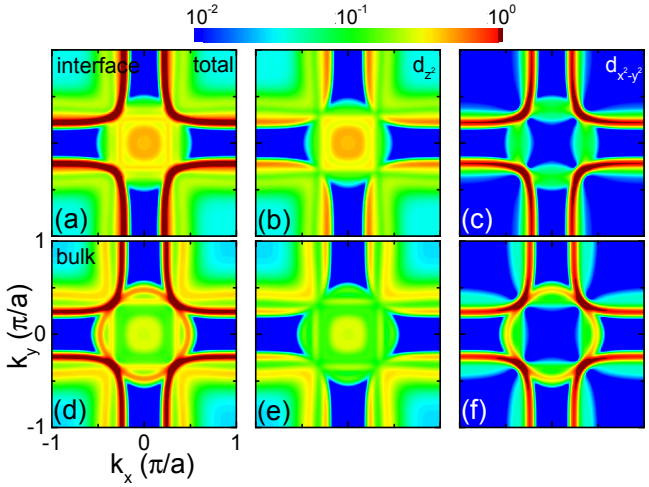

FIG. 3. The $\boldsymbol{k}_{\|}$- and orbital-resolved Fermi level local density of states (LDOS) in the absence of spin-orbit coupling for majority-spin Mn-*d* states at the interface (a-c) and in the bulk (d-f): total (a, d), d_{z^2} (b, e) and $d_{x^2-y^2}$ (c, f) orbital contributions. Contributions from the Mn-*d* t_{2g} orbitals are negligible due to the crystal field splitting. Minority-spin LDOS in the absence of spin-orbit coupling is zero due to half-metallicity of LSMO. Note that the color scale for LDOS is logarithmic.

To explore the origin of this region with enhanced transmission, we plot in Fig. 3 the $\boldsymbol{k}_{\|}$-resolved local density of states (LDOS) at the Fermi energy on the Mn sites. States at the Fermi level in LSMO derive mainly from the Mn-*d* orbitals, specifically those with e_g character, i.e., d_{z^2} and $d_{x^2-y^2}$. Comparing Fig. 3(b) and (e) with Fig. 2(a) we see that that the transmission derives mostly from d_{z^2} orbitals. This is due to d_{z^2} orbitals having an out-of-plane character and thus dispersive σ-bond-like coupling along the transport direction, in contrast to planar $d_{x^2-y^2}$ orbitals with small coupling along the transport direction. Importantly, we see from Fig. 3(a) that, even in the absence of SOC, there is a square-like feature inside the circular region surrounding $\boldsymbol{k}_{\|} = 0$ on the interfacial Mn sites. This feature coincides precisely with the region of enhanced transmission in Fig. 2(c). Furthermore, this feature is not present in the bulk of the LSMO, as shown in Fig. 3(d).

IV. DISCUSSION AND MODEL

Let us explore why the transmission in the **M** || **x** case is so strongly affected by the SOC effect, whereas the **M** || **z** case is essentially unchanged with respect to the transmission in the absence of SOC. While SOC formally makes electron spin no-longer a good quantum number, the half-metallic character of LSMO is, to a large extent, preserved, i.e. the density of minority-spin states at the Fermi level is negligibly small. Therefore we focus our attention on the effects of SOC which preserve spin.

For **M** || **z**, the effective spin-orbit Hamiltonian for Mn-*d* states is

$$H_{so} = \lambda \mathbf{L}\cdot\mathbf{S} = \lambda \begin{pmatrix} L_z & L_x + iL_y \\ L_x - iL_y & -L_z \end{pmatrix}, \qquad (2)$$

where λ is an effective SOC constant and L_x, L_y and L_z are the orbital angular momentum operators. As described above, we expect the largest effects on the transmission from SOC to come from spin-conserving matrix elements affecting the majority-to-majority spin channel, i.e. the upper left element in Eq. (2). Since the transmission is dominated by states with Mn-d_{z^2} character, and since $L_z|d_{z^2}\rangle = 0$, the SOC effect should be small for **M** || **z**. Comparing Figs. 2(a) and (b), this is clearly the case.

For **M** || **x**, on the other hand, the effective spin-orbit Hamiltonian reads

$$H_{so} = \lambda \mathbf{L}\cdot\mathbf{S} = \lambda \begin{pmatrix} L_x & iL_y - L_z \\ -iL_y - L_z & -L_x \end{pmatrix}. \qquad (3)$$

In this case, since $L_x|d_{z^2}\rangle \neq 0$, there are indeed expected to be non-negligible effects on the transmission due to SOC. In particular, L_x introduces spin-conserving matrix elements between states with d_{z^2} and d_{zy} orbital character.

While these considerations account for the apparent effect of SOC on the **M** || **x** case and not for the **M** || **z** case, it does not address the question of *why* this effect produces such a large TAMR effect. Why would coupling with the d_{zy} states, which belong to the t_{2g} manifold of the octahedral crystal field split Mn-*d* states and therefore lie a moderate distance below the Fermi level, produce such a large effect on the transmission of states at the Fermi level? To address this issue, we return to the phenomenon of the electric field at the interface which arises due to the polar mismatch between LSMO and STO. The electrostatic potential shift near the interface, as shown in Fig. 4(a), pushes all states upward with respect to the states deep inside the LSMO (compare to Fig. 4(c)). In fact, the shift in the potential is large enough to push some of the t_{2g} states at the interface above the main t_{2g} bulk bands, leading to a quasi-localization of these states at the interfacial layer. The

energetic proximity of these states to the d_{z^2} states at the Fermi level is now greatly increased and therefore one expects the SOC-induced interaction to be significant for the **M** || **x** case.

To see how the presence of these quasi-localized states can lead to a significant enhancement of the tunneling transmission we construct a simple one-dimensional tight-binding model. We consider two bands belonging to the majority-spin channel: a wide band and a narrow band, with on-site energies and nearest neighbor hopping parameters $\varepsilon_{z^2} = 0.8$ eV, $t_{z^2} = 1.0$ eV and $\varepsilon_{zy} = -1.2$ eV, $t_{zy} = 0.25$ eV, respectively, as shown in Fig. 5(a). These parameters approximate the d_{z^2}- and d_{zy}-like bands along the [001] direction of LSMO. Finally, SOC is included by introducing a matrix element $\lambda = 0.1$ eV between the d_{z^2} and d_{zy} orbitals, but only for the **M** || **x** case. A tunnel barrier is approximated by a break in the infinite one-dimensional chain across which the two separate bands are assumed to have (energy independent) matrix elements $V_{z^2} = 10^{-4}$ eV and $V_{zy} = 10^{-3}$ eV.

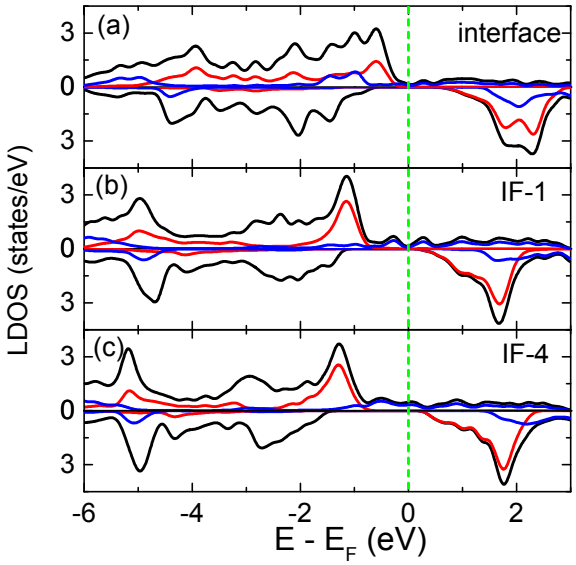

FIG. 4. Layer-resolved local density of states (LDOS) in the absence of spin-orbit coupling for MnO_2 layers (a) at the interface, (b) layer adjacent to the interface (IF-1) and (c) far away from the interface (IF-4). Majority-spin states are in the upper panels, and minority-spin states are in the lower panel. Black, red and blue curves correspond to MnO_2 total, Mn-t_{2g} and Mn-e_g states, respectively.

The transmission as a function of energy for this model can be computed using tight-binding Green's function techniques. [29] We find that changing the magnetization orientation from **M** || **z** to **M** || **x** leads to only a small increase in transmission above the top of the d_{zy} band, and the transmission near the Fermi-level is barely affected, as shown in Fig. 5(b). This result, however, neglects the electric field near the interface predicted from our first-principles calculations. We model this by shifting the on-site energies at the interface atom by $\delta V = 0.9$ eV, similar to what is seen for the LDOS in Fig. 4. With this shift, an interface-localized state is pushed outside of the bulk d_{zy} band. For **M** || **z**, this state plays no role in the transmission spectrum, as it is uncoupled from any bulk-like states [solid curve in Fig. 5(c)]. For **M** || **x**, on the other hand, this state is now coupled to the d_{z^2} bulk bands and appears as a strong resonance in the transmission [dotted curve in Fig. 5(c)]. For the parameters chosen the peak of this resonance is wide enough to lead to a noticeable increase in the transmission around the Fermi level compared to the **M** || **z** state, yielding a TAMR effect of 551%. It is clear, however, that depending on the position of this state the TAMR effect can be much larger. In the realistic 3D tunnel junction the in-plane dispersion of the interface quasi-localized states leads to $\boldsymbol{k}_{\|}$-dependent enhanced transmission for the **M** || **x** case: for some $\boldsymbol{k}_{\|}$ the resonance will be closer to E_F than others, yielding a cumulative enhancement of transmission and, therefore, a large net TAMR effect.

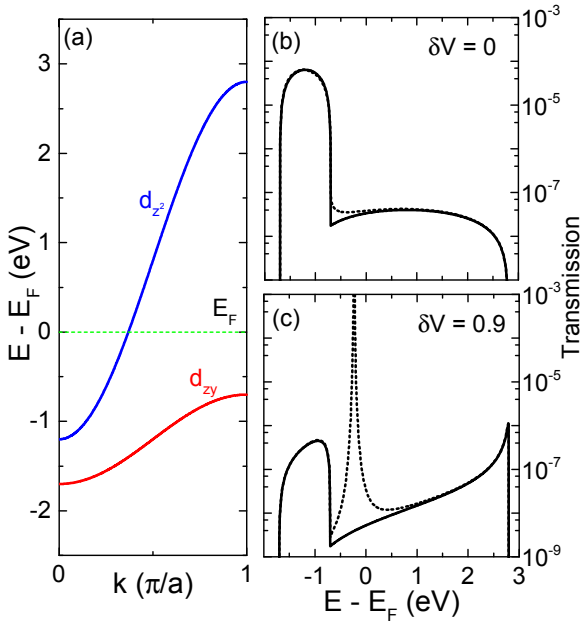

FIG. 5. (a) Model band structure of the majority spin d_{z^2} and d_{zy} states. Transmission across the model tunnel barrier (b) without and (c) with the local shift of the potential on the interfacial site is plotted for **M** || **z** (solid curve) and **M** || **x** (dotted curve).

V. OUTLOOK AND CONCLUSIONS

Previous experimental studies [30] of LSMO/STO superlattices revealed AMR effects of only ~4%, though these were for in-plane magnetizations and thick STO layers (tens of unit cells), well outside the tunneling regime we describe here. For experimental demonstration of the TAMR effect predicted here, it is critical that LSMO/STO/LSMO tunnel junctions are fabricated with thin STO barriers (only a few unit cells) and atomically

sharp interfaces. This can be achieved using modern thin-film deposition techniques, such as molecular beam epitaxy or pulsed laser deposition. Recently developed experimental techniques exist to probe buried LSMO/STO interfaces for the presence of the interface-specific features predicted by our calculations to originate from the polar mismatch.[31,32] Furthermore, the band alignment between LSMO and STO can be continuously controlled by sub-unit-cell deposition of a $SrMnO_3$ layer,[33] which in our case allows a shift of the Fermi energy and thus control of the magnitude of the TAMR effect (Fig. 5). Interface engineering can also be used to enhance magnetic properties of the interface,[34,35] and to control the interface resonant states which are known to play an important role in spin-dependent tunneling.[36] Furthermore, it is important to note that using only one magnetic electrode will generally suffice to observe TAMR. For LSMO specifically the effect relies on the fact that the majority-spin d_{z^2} orbital is the dominant channel for tunneling. The lead counter to LSMO, as well as the barrier, would need to be compatible with this. We therefore hope that our theoretical predictions will create interest among experimentalists to realize such a large TAMR.

In conclusion, we have demonstrated that LSMO/STO/LSMO tunnel junctions can exhibit a very large TAMR effect. We predict a ~500% change in tunneling resistance between in-plane and out-of-plane magnetization states. The origin of this effect stems from the half-metallic nature of the LSMO electrodes and the presence of quasi-localized interface states which are spin-orbit-coupled, depending on magnetization orientation, to the states at the Fermi level. This large magnetoresistance effect may be interesting as an alternative or complementary route to develop magnetic field sensors for magnetic data storage applications.

ACKNOWLEDGEMENTS

This research was supported by the National Science Foundation (NSF) through Materials Research Science and Engineering Center (MRSEC, grant no. DMR-1420645). Computations were performed at the University of Nebraska Holland Computing Center.

* E-mail: jdburton1@gmail.com
† E-mail: tsymbal@unl.edu

[1] I. Zutic, J. Fabian, and S. D. Sarma, Rev. Mod. Phys. **76**, 323 (2004).
[2] C. Chappert, A. Fert, and F. N. Van Dau, Nature Mater. **6**, 813 (2007).
[3] E. Y. Tsymbal, O. N. Mryasov, and P. R. LeClair, J. Phys.: Cond. Mat. **15**, R109 (2003).
[4] M. I. Katsnelson, V. Y. Irkhin, L. Chioncel, A. I. Lichtenstein, and R. A. de Groot, Rev. Mod. Phys. **80**, 315 (2008).
[5] J. H. Park, E. Vescovo, H. J. Kim, C. Kwon, R. Ramesh, and T. Venkatesan, Nature **392**, 794 (1998).
[6] M. Bowen, M. Bibes, A. Barthélémy, J.-P. Contour, A. Anane, Y. Lemaı□tre, and A. Fert, Appl. Phys. Lett. **82**, 233 (2003).
[7] W. Thomson, Proc. Roy. Soc. London **8**, 546 (1857).
[8] T. McGuire and R. Potter, IEEE Transactions on Magnetics **11**, 1018 (1975).
[9] A. Matos-Abiague and J. Fabian, Phys. Rev. B **79**, 155303 (2009).
[10] C. Gould, C. Rüster, T. Jungwirth, E. Girgis, G. M. Schott, R. Giraud, K. Brunner, G. Schmidt, and L. W. Molenkamp, Phys. Rev. Lett. **93**, 117203 (2004).
[11] H. Saito, S. Yuasa, and K. Ando, Phys. Rev. Lett. **95**, 086604 (2005).
[12] C. Ruster, C. Gould, T. Jungwirth, J. Sinova, G. M. Schott, R. Giraud, K. Brunner, G. Schmidt, and L. W. Molenkamp, Phys. Rev. Lett. **94**, 027203 (2005).
[13] J. Moser, A. Matos-Abiague, D. Schuh, W. Wegscheider, J. Fabian, and D. Weiss, Phys. Rev. Lett. **99**, 056601 (2007).
[14] L. Gao, X. Jiang, S.-H. Yang, J. D. Burton, E. Y. Tsymbal, and S. S. P. Parkin, Phys. Rev. Lett. **99**, 226602 (2007).
[15] A. N. Chantis, K. D. Belashchenko, E. Y. Tsymbal, and M. van Schilfgaarde, Phys. Rev. Lett. **98**, 046601 (2007).
[16] K. I. Bolotin, F. Kuemmeth, and D. C. Ralph, Phys. Rev. Lett. **97**, 127202 (2006).
[17] J. D. Burton, R. F. Sabirianov, J. P. Velev, O. N. Mryasov, and E. Y. Tsymbal, Phys. Rev. B **76**, 144430 (2007).
[18] N. Néel, S. Schröder, N. Ruppelt, P. Ferriani, J. Kröger, R. Berndt, and S. Heinze, Phys. Rev. Lett. 110, 037202 (2013).
[19] J.-J. Li, M.-L. Bai, Z.-B. Chen, X.-S. Zhou, Z. Shi, M. Zhang, S.-Y. Ding, S.-M. Hou, W. Schwarzacher, R. J. Nichols, and B.-W. Mao, J. Amer. Chem. Soc. 137, 5923 (2015).
[20] B. G. Park, J. Wunderlich, X. Martí, V. Holý, Y. Kurosaki, M. Yamada, H. Yamamoto, A. Nishide, J. Hayakawa, H. Takahashi, A. B. Shick, and T. Jungwirth, Nature Mater. 10, 347 (2011).
[21] Z. Fang, I. V. Solovyev, and K. Terakura, Phys. Rev. Lett. **84**, 3169 (2000).
[22] J. D. Burton and E. Y. Tsymbal, Phys. Rev. Lett. **106**, 157203 (2011).
[23] P. Giannozzi *et al.*, J. Phys.: Cond. Mat. **21**, 395502 (2009).
[24] J. P. Perdew, K. Burke, and M. Ernzerhof, Phys. Rev. Lett. **77**, 3865 (1996).
[25] J. D. Burton and E. Y. Tsymbal, Phys. Rev. B **82**, 161407 (2010).
[26] H. J. Choi and J. Ihm, Phys. Rev. B **59**, 2267 (1999).
[27] A. Smogunov, A. Dal Corso, and E. Tosatti, Phys. Rev. B **70**, 045417 (2004).
[28] A. Dal Corso, A. Smogunov, and E. Tosatti, Phys. Rev. B **74**, 045429 (2006).
[29] S. Datta, *Electronic Transport in Mesoscopic Systems* Cambridge University Press, Cambridge, England, 1995.
[30] L. M. Wang, J.-K. Lin, and J.-P. Shyu, Phys. Rev. B **74**, 184412 (2006).
[31] A. X. Gray *et al.*, EPL **104**, 17004 (2013).
[32] J. A. Mundy, Y. Hikita, T. Hidaka, T. Yajima, T. Higuchi, H. Y. Hwang, D. A. Muller, and L. F. Kourkoutis, Nature Comm. **5**, 3464 (2014).

[33] Y. Hikita, M. Nishikawa, T. Yajima, and H. Y. Hwang, Phys. Rev. B **79**, 073101 (2009).
[34] H. Yamada, Y. Ogawa, Y. Ishii, H. Sato, M. Kawasaki, H. Akoh, and Y. Tokura, Science **305**, 646 (2004).
[35] H. Boschker *et al*., Adv. Funct. Mater. **22**, 2235 (2012).
[36] E. Y. Tsymbal, K. D. Belashchenko, J. P. Velev, S. S. Jaswal, M. van Schilfgaarde, I. I. Oleynik, and D. A. Stewart, Prog. Mater. Sci. **52**, 401 (2007).